Pramana – J. Phys. (2016) 87: 72
DOI 10.1007/s12043-016-1285-8

Optical characteristics of transparent samarium oxide thin films deposited by the radio-frequency sputtering technique

A A ATTA[1,2,*], M M EL-NAHASS[2], KHALED M ELSABAWY[3,4], M M ABD EL-RAHEEM[1,5], A M HASSANIEN[6], A ALHUTHALI[1], ALI BADAWI[1] and AMAR MERAZGA[1]

[1]Department of Physics, Faculty of Science, Taif University, Taif 888, Saudi Arabia
[2]Department of Physics, Faculty of Education, Ain Shams University, Roxy 11757, Cairo, Egypt
[3]Materials Science Unit, Department of Chemistry, Faculty of Science, Tanta University, 31725 Tanta, Egypt
[4]Department of Chemistry, Faculty of Science, Taif University, Taif 888, Saudi Arabia
[5]Department of Physics, Faculty of Science, Sohag University, Sohag 82524, Egypt
[6]Department of Physics, Faculty of Science and Humanity Studies at Al-Quwayiyah, Shaqra University, Al-Quwayiyah 11971, Saudi Arabia
*Corresponding author. E-mail: aatta08@yahoo.com

MS received 8 November 2015; revised 23 December 2015; accepted 25 January 2016; published online 7 October 2016

Abstract. Transparent metal oxide thin films of samarium oxide (Sm_2O_3) were prepared on pre-cleaned fused optically flat quartz substrates by radio-frequency (RF) sputtering technique. The as-deposited thin films were annealed at different temperatures (873, 973 and 1073 K) for 4 h in air under normal atmospheric pressure. The topological morphology of the film surface was characterized by using atomic force microscopy (AFM). The optical properties of the as-prepared and annealed thin films were studied using their reflectance and transmittance spectra at nearly normal incident light. The estimated direct optical band gap energy (E_g^d) values were found to increase by increasing the annealing temperatures. The dispersion curves of the refractive index of Sm_2O_3 thin films were found to obey the single oscillator model.

Keywords. Transparent oxide; radio-frequency sputtering; optical properties; effect of annealing temperature.

PACS Nos 78.20.−e

1. Introduction

There have been extensive researches on the optical and electrical properties of the rare-earth (RE) transparent metal oxide (TMO) thin films, as they are often used in thin film optoelectronic devices, switching mechanism for logic devices, and memories [1–3]. They exhibit high resistivity, high dielectric constant and large optical band gap. They are used as potential candidates of high-k materials in the complementary metal oxide semiconductor (CMOS) devices [4,5]. Sm_2O_3 is a typical RE transparent metal oxide which can substitute SiO_2 in the CMOS devices because of its range of dielectric constant from 7 to 15, large band gap (4.33 eV) and high chemical and thermal stability with Si [6–8]. Sm_2O_3 thin film can be deposited by RF magnetron sputtering [9,10], electron beam evaporation [11], vacuum thermal evaporation [7], pulsed laser deposition (PLD) [12], atomic layer deposition (ALD) [6], metal-organic chemical vapour deposition (MOCVD) [13] and pyrolysis [14]. Among these methods, RF sputtering method is known to produce homogeneous and reproducible high-quality thin films of various types of materials, especially TMO materials. This method provides economical and efficient usage of evaporants and can be extended to industrial scales for device fabrication [15].

The optical constants play important roles in the research for modern optical devices because it is an important factor in optical communication. The determination of the optical properties of any material is essential to measure its ability to absorb and scatter light, and thus to evaluate its role for designing new optical devices. The refractive index (n) and dielectric constant (ε) of the semiconducting materials are very important in determining the optical properties of the

crystals. Knowledge of n is essential in the design of heterostructure lasers in optoelectronic devices as well as in solar cell applications [16,17].

Post-annealing treatment plays a critical role in the final structure and properties of the TMO thin films. Annealing treatment of TMO thin films in air, oxygen or nitrogen can improve the crystallinity and transmittance, but it can degrade the electrical properties due to the chemisorptions of O_2 or N_2 present at grain boundaries [18,19]. Empirical evidence has shown that TMO films must either be deposited at high temperature (>573 K) or undergo post-deposition thermal annealing to achieve the desired optical and electrical qualities [20–22]. The studies on the structure and optical properties of Sm_2O_3 thin films under different conditions are important to modify the microstructure and to develop their interesting technological applications. The prime aims of this work are to show how to deposit highly transparent Sm_2O_3 thin films by RF sputtering and to study the effect of annealing temperature on the morphological and optical properties of Sm_2O_3 thin films.

2. Experimental techniques

Sm_2O_3 thin films in this study were deposited on precleaned fused optically flat quartz substrates using Univex 350 sputtering unit with RF power model Turbo drive TD20 classic (Leybold) and thickness monitor model Inficon AQM 160. The ceramic Sm_2O_3 target, from Cathey Advanced Materials Limited, was used as a sputtering source. The sputtering chamber was evacuated to a base pressure of 2×10^{-6} Torr and was back-filled with mixture of 98% pure argon + 2% pure O_2 and up to the sputtering pressure of 2×10^{-2} Torr and the sputtering pressure was maintained constant throughout the coating. Prior to deposition the substrates were cleaned using a 10% by volume solution of hydrofluoric acid followed by a rinse in deionized water. The target-substrate distance was 10 cm with 65° angle. The sccm standard was maintained at 20 cm^3/min with 2 rpm substrate rotation and power of 150 W. The rate of deposition was 2 nm/min. The thickness of the thin films was determined accurately after deposition by using multiple-beam Fizeau fringes in reflection [23]. Sm_2O_3 thin film with 230 nm thickness was annealed at 873 K, 973 K and 1073 K for 4 h in air under normal atmospheric pressure.

The non-contact mode of a high-resolution atomic force microscope (AFM) of model (Veeco-di Innova Model-2009-AFM-USA) was used for the topographical images of the film surface. The acquired AFM images were used to determine the roughness of the films and the sizes of the crystallite.

Transmittance, $T(\lambda)$, and reflectance, $R(\lambda)$, of the as-deposited and annealed films were measured at normal incidence in 190–2500 nm wavelength range using double beam spectrophotometer (JASCO model V-670 UV–Vis–NIR) attached with constant angle specular reflection attachment (5°), to determine the spectral behaviour of the optical constants and to deduce some optical parameters of the Sm_2O_3 thin film. The spectral data obtained directly from the spectrophotometer were converted to absolute values by making a correction to eliminate the absorbance and reflectance of the substrate. The absolute values of $T(\lambda)$ and $R(\lambda)$ are given by [24]

$$T = \left(\frac{I_{\mathrm{ft}}}{I_{\mathrm{q}}}\right)(1 - R_{\mathrm{q}}), \tag{1}$$

where I_{ft} and I_{q} are the intensities of light passing through the film-quartz system and that passing through the reference quartz, respectively and R_{q} is the reflectance of the quartz substrate, and

$$R = \left(\frac{I_{\mathrm{fr}}}{I_{\mathrm{m}}}\right) R_{\mathrm{m}}(1 + [1 - R_{\mathrm{q}}]^2) - T^2 R_{\mathrm{q}}, \tag{2}$$

where I_{m} is the intensity of light reflected from the reference mirror, I_{fr} is the intensity of light reflected from the sample and R_{m} is the reflectance of the mirror.

In order to calculate the optical constants, refractive index (n) and the absorption index (k) of the films at different wavelengths, we use the following equations [25,26]:

$$\alpha = \frac{1}{t}\ln\left[\frac{(1-R)^2}{2T} + \sqrt{\frac{(1-R)^4}{4T^2} + R^2}\right], \tag{3}$$

$$k = \frac{\alpha\lambda}{4\pi}, \tag{4}$$

$$n = \left(\frac{1+R}{1-R}\right) + \sqrt{\frac{4R}{(1-R)^2} - k^2}, \tag{5}$$

where α is the absorption coefficient and t is the film thickness. The experimental errors in the calculated values of n and k are with accuracy better than ±4% [27]; taking into account, the experimental errors in measuring the film thickness as ±2% and in measuring T and R as ±1%.

3. Results and discussion

Figure 1 shows 3D-AFM-surface topology of the as-deposited and annealed Sm_2O_3 thin films with 230 nm

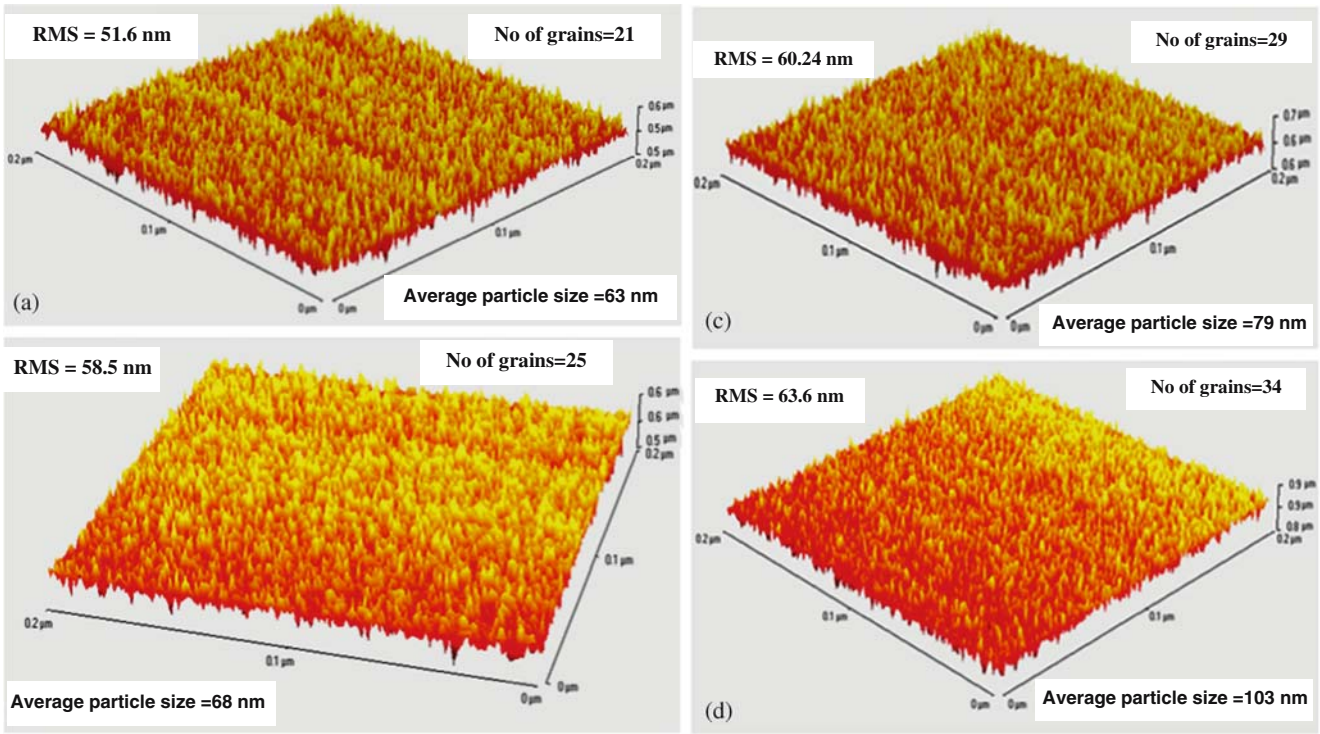

Figure 1. AFM images ($2 \times 2\ \mu m^2$) showing the surface morphology of Sm_2O_3 thin films (**a**) as-deposited and annealed for 4 h at (**b**) 873 K, (**c**) 973 K and (**d**) 1073 K.

thickness using applying tapping mode. The smoothness of the surface in terms of root mean square surface (RMS) roughness is found to increase from 51.6 nm for the as-deposited film to 63.6 nm after annealing at 1073 K and the obtained average particle size is also increased from 63 nm for the as-deposited film to 103 nm after annealing at 1073 K. The increase in particle size was associated with the tendency of the particles to grow by fusion of adjacent particles when sufficient energy for the surface rearrangement is provided by annealing [28]. Also the number of grains present on the surface of the investigated sample ($0.2 \times 0.2\ \mu m^2$) are found to increase from 21 for the as-deposited film to 34 after annealing at 1073 K. This increase in the number of grains means that the annealing makes as splitter to the grain size in the scanned area.

Figure 2 displays 3D-AFM-surface mapping for the as-deposited and annealed Sm_2O_3 thin films. From figure 2a one can conclude that the majority of heights distribution lies between 0.51 and 0.52 μm (green zone area), maximum height represented by red colour ($\sim$2% of the scanned area) is found to be 0.54 μm and the minimum height ($\sim$0.49–0.50 μm) occupies blue colour area. The estimated heights gradient for each colour for the as-deposited and annealed (figures 2b, 2c and 2d) Sm_2O_3 thin films are tabulated in table 1.

Figures 3a and 3b illustrate transmittance, $T(\lambda)$, and reflectance, $R(\lambda)$, for the as-deposited and annealed Sm_2O_3 thin film of 230 nm thickness. At longer wavelength (2500 nm), the figure shows that the transmittance increases from 94% for the as-deposited film to 96% after annealing at 1073 K for 4 h. In the absorption region ($\lambda < 400$ nm), the transmittance spectra of the annealed films are slightly shifted to lower wavelength (blue shift). Such shifts are related to blue shift change in the optical band gap of the annealed Sm_2O_3 thin films.

The absorption coefficient α for the as-deposited and annealed Sm_2O_3 thin films can be used to estimate the type of transition and the optical band-gap enery according to Tauc's relationship [26]

$$(\alpha h\nu) = B(h\nu - E_g)^r, \tag{6}$$

where E_g is the optical band-gap energy, B is a constant and r is a constant which depends on the probability of transition; $r = 1/2$ and $3/2$ for direct allowed and forbidden transitions, respectively, $r = 2$ and 3 for indirect allowed and forbidden transitions, respectively. The dependence of $(\alpha h\nu)^{1/r}$ on photon energy ($h\nu$) was plotted for different values of r. The best fit was obtained for $r = 1/2$ and displayed in figure 4; this result pointed out that the transitions are direct allowed transitions. The direct band-gap estimation can be found

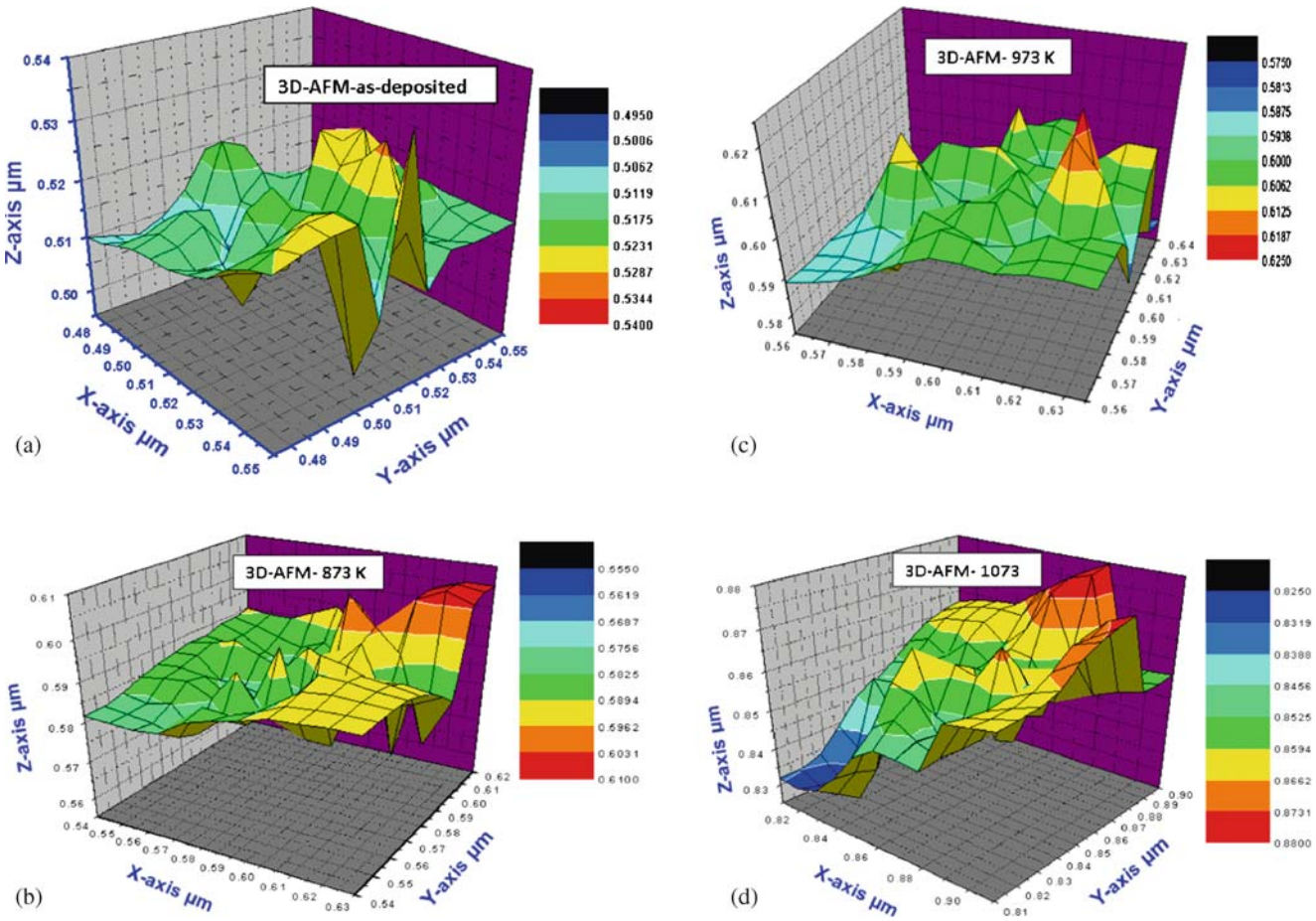

Figure 2. 3D-visualized image of plank for area 0.08 × 0.08 μm^2 for Sm_2O_3 thin films (**a**) as-deposited and annealed for 4 h at (**b**) 873 K, (**c**) 973 K and (**d**) 1073 K.

Table 1. Height gradients of different colours in 3D-visualized image for the scanned area (0.08×0.08 μm^2) for the as-deposited and annealed Sm_2O_3 thin films.

Height gradient	As-deposited film (μm)	Annealed film at 873 K (μm)	Annealed film at 973 K (μm)	Annealed film at 1073 K (μm)
Green zone area	0.51–0.52	0.58–0.59	0.59–0.61	0.85–0.86
Red zone area	0.53–0.54	0.60–0.61	0.62–0.63	0.87–0.89
Blue zone area	0.51–0.55	0.56–0.57	0.58–0.59	0.83–0.84

by the extrapolated linear regression of the curve resulting from a plot of $(\alpha h\nu)^2$ vs. photon energy $(h\nu)$. The results indicate that optical band-gap values vary with the annealing temperature. The estimated values of the direct optical gap show an obvious increase (blue shift) from 4.51 eV for the as-deposited film to 4.69 eV, 4.87 eV and 5.02 eV after annealing at 873 K, 973 K and 1073 K, respectively. This increase of optical band gap may be due to an improvement in the crystalline structure of the film, because if the film becomes more polycrystalline the band gap is broadened by a decrease in band gap defects [19]. In addition, the decrease of optically derived surface roughness for annealed films can also be connected to changes in film structure linked to a decrease in voids [29].

Also, the increase of the optical band gap was explained by Burstein–Moss (BM) effect due to the increased carrier concentration [30]. It was well known that band-gap widening occurred in heavily doped semiconductors [30–32]. Band-gap widening is referred to as the BM

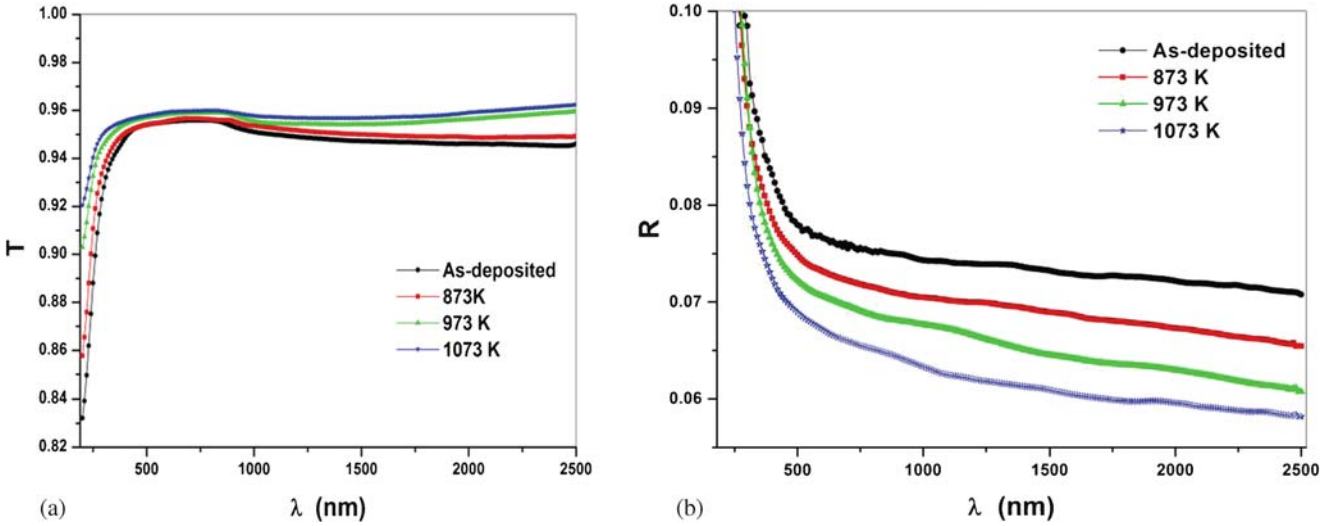

Figure 3. (**a**) The optical transmittance $T(\lambda)$ for the as-deposited and annealed Sm_2O_3 thin films and **(b)** the optical reflectance $R(\lambda)$ for the as-deposited and annealed Sm_2O_3 thin films.

effect, the conduction band becomes significantly filled at high doping concentration and the lowest energy states in the conduction band are blocked. After annealing, the optical band gap and the carrier concentration were increased. The increase of carrier concentration by annealing is due to the generation of oxygen vacancies due to thermal energy.

Figure 5 shows the real part of the refractive index, $n(\lambda)$, for the as-deposited and annealed Sm_2O_3 thin films. This figure shows that the refractive index of the as-deposited films decreased by increasing the wavelength from approximately 2.26 at $\lambda = 200$ nm to 1.72 at $\lambda = 2500$ nm.

According to the classical dispersion theory, the spectral behaviour of $n(\lambda)$ in the transparent region (negligible damping) can be described by using the single-oscillator model of the form [33,34]:

$$\frac{1}{n^2-1} = \frac{E_o}{E_d} - \frac{1}{E_o E_d}(h\nu)^2, \tag{7}$$

where $h\nu$ represents the photon energy, E_o is energy of the oscillator and E_d is the dispersion energy which is a measure of the strength of the interband optical transitions. The calculated values of the dispersion parameters as well as the infinite frequency dielectric constant, ε_∞, can be obtained by plotting $(n^2-1)^{-1}$ against $(h\nu)^2$ for the as-deposited and annealed Sm_2O_3 thin films as shown in figure 6. The calculated value of ε_∞ is found

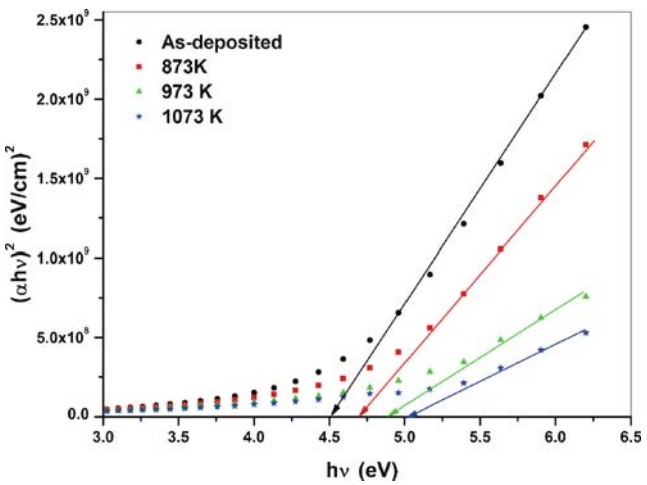

Figure 4. The relation between $(\alpha h\nu)^2$ and photon energy $(h\nu)$ for the as-deposited and annealed Sm_2O_3 thin films.

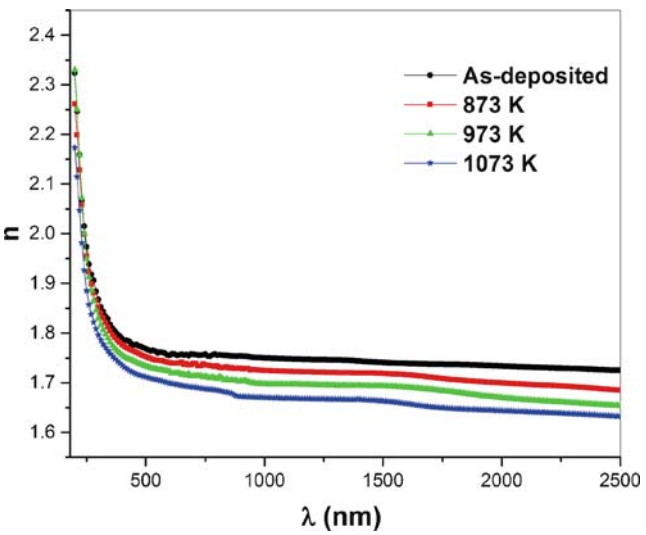

Figure 5. The spectral behaviour of the real part of the refractive index, $n(\lambda)$, for the as-deposited and annealed Sm_2O_3 thin films.

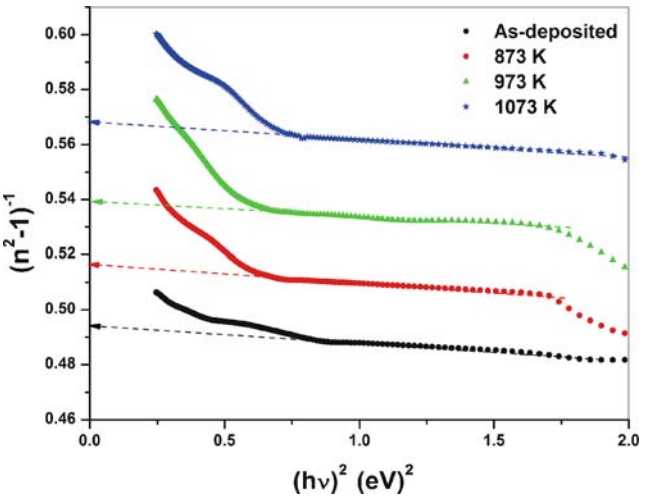

Figure 6. The relation between $(n^2-1)^{-1}$ and $(h\nu)^2$ for the as-deposited and annealed Sm_2O_3 thin films.

to decrease from 3.03 for the as-deposited Sm_2O_3 thin film to 2.76 after annealing at 1073 K, the calculated value of E_d is found to decrease from 19.46 eV for the as-deposited Sm_2O_3 thin film to 17.76 eV after annealing at 1073 K and the calculated value of E_o is found to increase from 9.59 eV for the as-deposited Sm_2O_3 thin film to 10.07 eV after annealing at 1073 K. The obtained dispersion parameters of the as-deposited and annealed Sm_2O_3 thin films are listed in table 2.

A significant success of Wemple and Di Domenico model is that it relates the dispersion energy (E_d) to other physical factors of the material through the following empirical relationship [33,34]:

$$E_d = \beta N_c Z_a N_e, \tag{8}$$

where N_c is the coordination number of the cation nearest-neighbour to the anion, Z_a is the formal chemical valency of the anion, N_e is the effective number of valence electrons per anion and β is a constant which takes the value (0.37 ± 0.04 eV) for covalently bonded crystalline and amorphous chalcogenides and takes the value (0.26 ± 0.04 eV) for halides and most oxides with a more ionic structure. $N_c = 4$ for the investigated compound Sm_2O_3. Considering the formal chemical valency of the anion $Z_a = 2$ and N_e the corresponding numbers of valence electrons, i.e. 4, 6, for Sm and O atoms, respectively, we get $N_e = 8$ [33,34]. Taking the experimental value of E_d for the as-deposited film ($E_d = 19.46$ eV) we get the calculated value of β for the as-deposited film ($\beta = 0.3$ eV).

Furthermore, the dispersion theory describes the variation of n^2 vs. λ^2 to estimate the lattice dielectric constant (ε_L) by taking into account the contribution of the free charge carriers and the lattice vibration modes of the dispersion. The relation between the real dielectric constant (ε_1) and λ^2 in the transparent region can be obtained by the following relation [35]:

$$\varepsilon_1 = n^2 = \varepsilon_L - \frac{e^2 N}{4\pi^2 \varepsilon_o m^* c^2}\lambda^2, \tag{9}$$

where ε_L is the lattice dielectric constant, e is the electronic charge, ε_o is the permittivity of free space and N/m^* is the ratio of the free carrier concentration to the free carrier effective mass. Figure 7 shows the relation between n^2 and λ^2 for the as-deposited and annealed Sm_2O_3 thin films. The figure shows the linear dependence of n^2 on λ^2 at longer wavelengths for the as-deposited and annealed Sm_2O_3 thin films. Extrapolating this linear part to zero wavelength gives the value of ε_L and from the slope of this linear part the ratio N/m^* can be calculated. The estimated values of ε_L and N/m^* are listed in table 2.

According to the Drude theory, at very low frequencies the optical properties of semiconductors exhibit a metal-like behaviour, while at very high frequencies their optical properties are like those of insulators. The characteristic frequency at which the material changes from metallic to dielectric is called the plasma frequency ω_p, which is defined as that frequency at which the real part of the dielectric function vanishes ($\varepsilon_1(\omega_p) = 0$) [36]. By using Drude model, the plasma frequency (ω_p) is connected to the density of the free charge carriers (N) by the relation [37,38]:

$$\omega_p = \left(\frac{e^2 N}{\pi\, c^2 m^*}\right)^{1/2} (\mathrm{cm}^{-1}). \tag{10}$$

The estimated values of ω_p for the as-deposited and annealed Sm_2O_3 thin films are listed in table 2.

Table 2. Optical parameters of the as-deposited and annealed Sm_2O_3 thin films.

	E_g^{opt}(eV)	E_o (eV)	E_d (eV)	ε_∞	ε_L	N/m^* (10^{46} g^{-1} cm^{-3})	ω_p (cm^{-1})
As-deposited film	4.51	9.59	19.46	3.03	3.06	1.60	1141.8
Annealed at 873 K	4.69	9.64	18.72	2.94	2.98	2.65	1469.5
Annealed at 973 K	4.87	10	18.55	2.85	2.88	2.85	1523.9
Annealed at 1073 K	5.02	10.07	17.76	2.76	2.77	2.06	1295.6

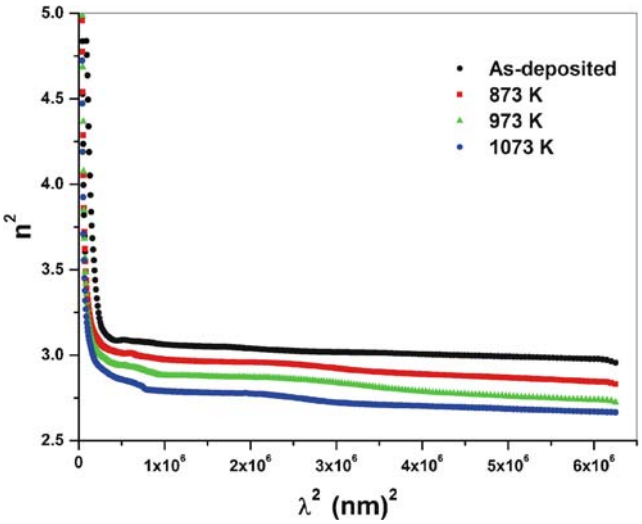

Figure 7. The relation between n^2 and λ^2 for the as-deposited and annealed Sm_2O_3 thin films.

4. Conclusion

The effect of annealing on the structural and optical properties of Sm_2O_3 thin films prepared by RF sputtering was studied. Atomic force microscope (AFM) was used to investigate the surface topology of the as-deposited and annealed Sm_2O_3 thin films. The average particle size was found to increase from 63 nm for the as-deposited film to 103 nm after annealing the film at 1073 K. The direct optical band-gap enery was found to slightly increase from $E_g^d = 4.51$ eV for the as-deposited film to $E_g^d = 5.02$ eV after annealing the film at 1073 K. The blue shift of the optical band gap was explained by Burstein–Moss (BM) effect. The classical single oscillator model and Drude model of free carriers' absorption were used for the analysis of refractive index dispersion, in the normal dispersion range. By using Drude model of free carriers' absorption, the calculated values of N/m^* and plasma frequency (ω_p) were found to change by annealing temperature.

Acknowledgements

Authors gratefully acknowledge Taif University (project #1-435-3629) for the financial assistance and facilitation of our study.

References

[1] B Renganathan, D Sastikumar, R Srinivasan and A R Ganesan, *Mater. Sci. Eng. B* **186**, 122 (2014)
[2] C Constantinescu, V Ion, A C Galca and M Dinescu, *Thin Solid Films* **520**, 6393 (2012)
[3] H Yang, H Wang, H M Luo, D M Feldmann, P C Dowden, R F DePaula and Q X Jia, *Appl. Phys. Lett.* **92**, 062905 (2008)
[4] M Fanciulli and G Scarel, Rare earth oxide thin film: Growth, characterization, and applications, *Topics in applied physics* (Springer, Berlin, 2007) Vol. 106, pp. 1–14
[5] G Scarel, A Debernardi, D Tsoutsou, S Spiga, S C Capelli, L Lamagna, S N Volkos, M Alia and M Fanciulli, *Appl. Phys. Lett.* **91**, 102901 (2007)
[6] J Päiväsaari, M Putkonen and L Nkknistö, *Thin Solid Films* **472**, 275 (2005)
[7] A A Dakhel, *J. Alloys Compd.* **365**, 233 (2004)
[8] T M Pan, C C Huang, S X You and C C Yeh, *Solid State Lett.* **11**, G62 (2008)
[9] T M Pan and C C Huang, *Appl. Surf. Sci.* **256**, 7186 (2010)
[10] M H Wu, C H Cheng, C S Lai and T M Pan, *Sensor. Actuat. B: Chem.* **138**, 221 (2009)
[11] M K Jayaraj and C P G Vallabhan, *Thin Solid Films* **197**, 15 (1991)
[12] D Yang, L J Xue and R A B Devine, *J. Appl. Phys.* **93**, 9389 (2003)
[13] K Shalini and S Shivashankar, *Bull. Mater. Sci.* **28**, 49 (2005)
[14] H Ono and T Katsumata, *Appl. Phys. Lett.* **78**, 1832 (2001)
[15] W Wohlmuth and I Adesida, *Thin Solid Films* **479**, 223 (2005)
[16] M A Yıldım, Y Akaltun and A Ateş, *Solid State Sci.* **14**, 1282 (2012)
[17] A Alhuthali, M M El-Nahass, A A Atta, M M Abd El-Raheem, K M Elsabawy and A M Hassanien, *J. Lumin.* **158**, 165 (2015)
[18] L B Duan, X R Zhao, J M Liu, W C Geng, H Y Xie and H N Sun, *Phys. Scr.* **85**, 035709 (2012)
[19] Y J Zhang, Z T Liu, D Y Zang, X S Che, L P Feng and X X Bai, *J. Phys. Chem. Solids* **74**, 1672 (2013)
[20] J A Stoke, J D Beach, W C Bradford and T R Ohno, *Thin Solid Films* **562**, 254 (2014)
[21] P Dongliang, S Jiang and W Wanlu, *Chin. Phys. Lett.* **10**, 189 (1993)
[22] X Wu, W P Mulligan and T J Coutts, *Thin Solid Films* **286**, 274 (1996)
[23] S Tolansky, *Multiple-beam interferometry surface and films* (Oxford University Press, London, 1978)
[24] M M El-Nahass, *J. Mater. Sci.* **27**, 6597 (1992)
[25] M Di Giulio, G Micocci, R Rella, P Siciliano and A Tepore, *Phys. Status Solidi A* **136**, K101 (1993)
[26] M M El-Nahass, A A Atta, M M Abd El-Raheem and A M Hassanien, *J. Alloys Compd.* **585**, 1 (2014)
[27] I Konstantinov, T Babeva and S Kitova, *Appl. Opt.* **37**, 4260 (1998)
[28] X Zhang, X Sun, H Huang, X Wang, Y Huang and X Ren, *Appl. Phys. Lett.* **104**, 061110 (2014)
[29] E Çetinörgü, S Goldsmith, Y Rosenberg and R L Boxman, *J. Non-Cryst. Solids* **353**, 2595 (2007)
[30] S C Jain, J M McGregor and D J Roulston, *J. Appl. Phys.* **68**, 3747 (1990)
[31] C E Kim, P Moon, S Kim, J Myoung, H W Jang, J Bang and I Yun, *Thin Solid Films* **518**, 6304 (2010)

[32] M Gulen, G Yildirim, S Bal, A Varilci, I Belenli and M Oz, *J. Mater. Sci: Mater. Electron.* **24**, 467 (2013)
[33] S H Wemple and M DiDomenico Jr, *Phys. Rev. B* **3**, 1338 (1971)
[34] S H Wemple, *Phys. Rev. B* **7**, 3767 (1973)
[35] E D Palik, *Handbook of optical constants of solids* (Academic Press Handbook, New York, 1985)
[36] García Solé, L E Bausá and D Jaque, An introduction to the optical spectroscopy of inorganic solids (John Wiley & Sons Ltd, 2005)
[37] E Feigenbaum, K Diest and H A Atwater, *Nano Lett.* **10**, 2111 (2010)
[38] R J Bell, M A Ordal and R W Alexander Jr, *Appl. Opt.* **24**, 3680 (1985)